Lattice dynamics of orthorhombic perovskite yttrium manganite, $YMnO_3$

2009 J. Phys.: Condens. Matter 21 355402

(http://iopscience.iop.org/0953-8984/21/35/355402)

J. Phys.: Condens. Matter **21** (2009) 355402 (7pp) doi:10.1088/0953-8984/21/35/355402

Lattice dynamics of orthorhombic perovskite yttrium manganite, $YMnO_3$

Mala N Rao[1], Nupinderjeet Kaur[2], S L Chaplot[1], N K Gaur[3] and R K Singh[4]

[1] Solid State Physics Division, Bhabha Atomic Research Centre, Mumbai-400085, India
[2] Department of Physics, Indian Institute of Technology, New Delhi-110016, India
[3] Department of Physics, Barkatullah University, Bhopal-462026, India
[4] School of Basic Sciences, MATS University, Raipur-492002, India

E-mail: mala@barc.gov.in

Received 20 January 2009, in final form 10 July 2009
Published 10 August 2009
Online at stacks.iop.org/JPhysCM/21/355402

Abstract

The lattice dynamics of yttrium manganite ($YMnO_3$) has been investigated by means of a shell model with pair-wise interionic interaction potential. The experimental data of crystal structure and Raman and infrared frequencies compare well with the lattice dynamical calculations. The phonon dispersion curves found along three high symmetry directions and the density of states of $YMnO_3$ have also been calculated from this model. The computed phonon density of states is used to derive the macroscopic thermodynamic quantities like the Debye temperature and specific heat. The crystal structure data computed from this model are in good agreement with the available experimental data measured by neutron powder diffraction. We have made a comparative study of the structures derived from the potential model calculations for both $LaMnO_3$ and $YMnO_3$. Symmetry vectors obtained through group theoretical analysis at the zone centre point were employed to classify the phonon frequencies obtained into their irreducible representations. The computed Raman and infrared frequencies have shown good agreement with the measured data.

1. Introduction

The theoretical understanding of manganese oxides [1, 2] is among the most challenging current areas of research in condensed matter physics. An extensive study of manganese oxides has been performed with structures of pseudo-cubic [3–6] and layered perovskites [7, 8] and pyrochlore [9, 10] for wide compositions from the viewpoints of exotic spin–charge coupled phenomena. The investigation of manganites is among the main areas of research within the field of strongly correlated electrons. After several theoretical efforts in recent years, mainly guided by the computational and mean-field studies of realistic models, considerable progress has been achieved in understanding the physical properties of these compounds. These materials are currently being investigated by a sizeable fraction of condensed matter scientists and their popularity is reaching levels comparable to that of the high temperature superconductors.

Rare earth manganese oxides, $RMnO_3$, form a broad class of transition metal oxides exhibiting a wide range of exotic galvanomagnetic, magnetic, electronic and optical properties [11, 12]. The rare earth manganites, $RMnO_3$, crystallize in two different crystallographic structures depending on the size of the ionic radius of the rare earth elements. The compounds with large ionic radii, R = La, Pr, Nd, Sm, Eu, Gd, Tb and Dy crystallize in the orthorhombic [13] perovskite structure of space group $Pnma$, whereas those with smaller ionic radii, R = Ho, Er, Tm, Yb, Lu and Y, have the hexagonal structure [14] with space group $P6_3cm$. However, upon annealing under high pressures, hexagonal (h-) $YMnO_3$ can be converted to its metastable orthorhombic phase. The huge interest in this family of strongly correlated systems has mostly been focused on the orthorhombic manganites, which exhibit colossal magnetoresistivity [15].

The crystal structure of orthorhombic (o-) $YMnO_3$ has been determined by various authors using neutron diffraction [14, 16, 17]. Its magnetic structure has also been studied by means of neutron diffraction experiments [14, 17]. $YMnO_3$ exhibits an incommensurate antiferromagnetic transition at around $T_N = 40$ K and the ferroelectric transition [18] at

Table 1. The potential parameters used in the models.

$LaMnO_3$ [28]			o-$YMnO_3$		
Ion	Effective charge (e)	Effective radius (Å)	Ion	Effective charge (e)	Effective radius (Å)
La	1.68	1.7474	Y	2.75	1.99
Mn	1.62	1.0801	Mn	1.57	1.11
O	−1.1	1.7976	O	−1.44	1.81
Oxygen shell charge = $-2.24e$			Oxygen shell charge = $-2.0e$		
Shell–core force constant = 142 eV $Å^{-2}$			Shell–core force constant = 140 eV $Å^{-2}$		

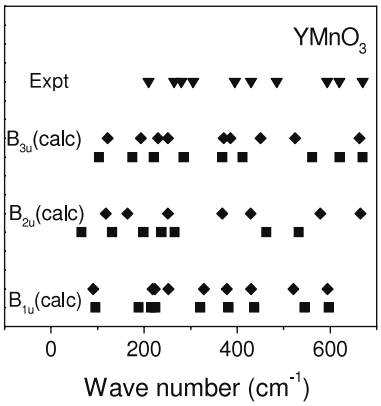

Figure 1. Comparison of the calculated (squares, this work; diamonds, from [24]) infrared active phonon frequencies and mode assignments with available experimental data [25] (triangles).

lower temperature $T_{FE} \sim 31$ K. The Raman active phonons in the orthorhombic perovskite $YMnO_3$ (and $LaMnO_3$) have been studied [19] for various scattering configurations and compared with calculated values from the lattice dynamical shell model [19]. These theoretical results are in good agreement with high frequency modes involving mainly oxygen motions, while the agreement is poor for the low frequency modes involving mainly Y (La) vibrations. Furthermore, the Raman phonons were employed as a probe of disorder, fluctuations and local structure in doped and undoped o-$RMnO_3$ by Martin-Carron *et al* [20]. Iliev *et al* have also studied Raman scattering of mixed valence manganites [21] as well as the variation of these phonon frequencies [22] with R ionic radius, whereas Laverdiere *et al* [23] investigated the temperature dependent Raman spectra of o-$YMnO_3$. Gupta and Ashdhir [24] applied a force-constant model to predict the Raman and infrared frequencies of o-$YMnO_3$. Limited information on the infrared phonons of orthomanganites is available in a work by Subba Rao *et al* [25] and in a recent work by Kim *et al* [26]. The thermodynamic properties of h-$YMnO_3$ have been assessed by Chen *et al* [27]. These authors have concluded that although their optimization results agree well with most of the experimental data for h-$YMnO_3$, the need for a complete thermodynamic description of the Mn–Y–O system is recommended by them [27].

In this paper, we have aimed to provide a microscopic interpretation of the structural, vibrational and thermodynamic properties of o-$YMnO_3$.

Table 2. Comparison between the experimental [16, 30] (at 14 K for $LaMnO_3$ and 295 K for o-$YMnO_3$) and calculated structural parameters (at 0 K). For the space group *Pnma*, Y (La), Mn and O1 and O2 atoms are located at (x, 0.25, z), (0, 0, 0), (x, 0.25, z) and (x, y, z), respectively, and their symmetry equivalent positions.

	$LaMnO_3$		$YMnO_3$	
	Experimental [30]	Calculated [28]	Experimental [16]	Calculated (this work)
a (Å)	5.739	5.616	5.8029	5.599
b (Å)	7.672	7.789	7.3643	7.506
c (Å)	5.532	5.503	5.2418	5.264
V ($Å^3$)	243.580	240.7	224.007	221.2
s	0.0367	0.0203	0.1016	0.0617
R (La/Y)				
x	0.549	0.541	0.5855	0.571
z	0.008	0.007	0.0181	0.011
B ($Å^2$)	0.32	0.12	0.87	0.47
Mn				
B ($Å^2$)	0.37	0.17	1.03	0.82
O1				
x	0.487	0.476	0.4660	0.453
z	0.575	0.577	0.6093	0.613
B ($Å^2$)	0.41	0.30	0.46	0.47
O2				
x	0.307	0.292	0.3266	0.317
y	0.038	0.041	0.0520	0.059
z	0.226	0.206	0.2005	0.193
B ($Å^2$)	0.45	0.31	0.90	0.61

2. Lattice dynamics computations

Previously, we have studied $LaMnO_3$ employing a shell model [28] with seven parameters based on an interatomic potential [29] consisting of the long-range Coulomb and the short-range interaction terms:

$$V(r) = \left\{\frac{e^2}{4\pi\varepsilon_o}\right\}\left\{\frac{Z(k)Z(k')}{r}\right\} + a\exp\left\{\frac{-br}{R(k)+R(k')}\right\} \quad (1)$$

where $a = 1822$ eV and $b = 12.364$. $Z(k)$ and $R(k)$ are the effective charge and radius parameters associated with atoms of type k. The polarizability of the oxygen ions was modelled using the shell model, where a massless shell is linked to the core by the harmonic interactions. We have

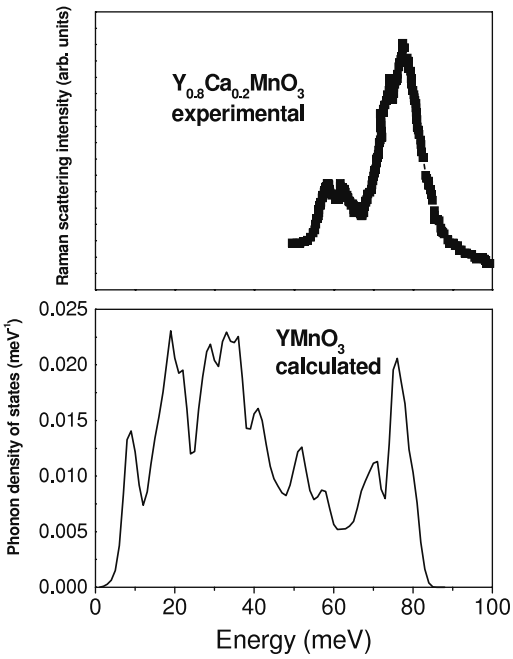

Figure 2. The calculated total one-phonon density of states for o-$YMnO_3$ compared with the Raman spectrum [31] for $Y_{0.8}Ca_{0.2}MnO_3$.

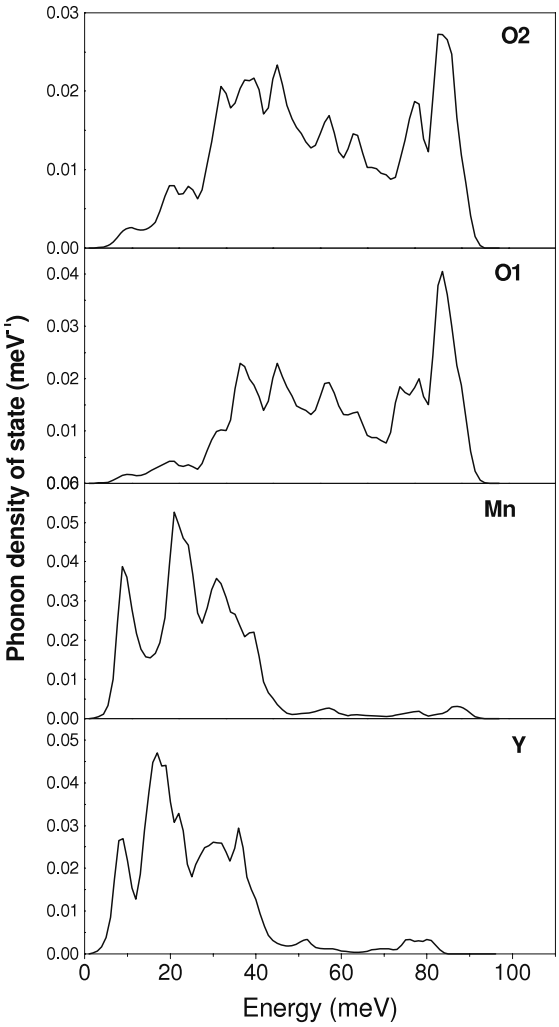

Figure 3. The calculated partial density of states for various atoms of o-$YMnO_3$.

investigated the crystal structure, phonon density of states, Raman frequencies, Debye temperatures, specific heat and phonon dispersion curves of o-$YMnO_3$ using this shell model. Earlier calculations [19, 24] have employed more complex lattice dynamical models, while we have used a simpler model with fewer adjustable parameters. The deviations from the ideal perovskite structure are larger for o-$YMnO_3$ and smaller for $LaMnO_3$; it is thus interesting to see how the model parameters need to change to take these into account.

The calculations reported in this paper have been performed using the computer program DISPR [29]. The structural parameters were relaxed to reach a minimum in the total potential energy. The optimized parameters of the potential (as shown in table 1), as obtained through this procedure, give nearly vanishing forces on all the atoms, crystal structure close to that determined by diffraction experiments, as well as real eigenvalues of the dynamical matrix.

The calculated density of states (as per the procedure given in [29]) has been used to evaluate the specific heat at constant volume (C_V) as a function of temperature.

3. Results and discussion

3.1. Structure

The calculated cell parameters and atomic coordinates with the optimized parameters of o-$YMnO_3$ are listed in table 1 and their respective experimental neutron diffraction data [16] are listed in table 2. It is noticed from the table that the computed values of lattice parameters as well as the fractional coordinates are in good agreement with experimental data [16, 30]. The calculated lattice parameters differ by 1.9% on average from the experimentally determined data [16, 30] at room temperature, similar to our earlier studies on $LaMnO_3$ [28]. Additionally, in going from the lanthanum to yttrium manganite, the increase in the spontaneous orthorhombic strain parameter, defined as $s = 2(a-c)/(a+c)$, is suitably reproduced by the potential model. The computed values of these lattice (a, b, c, V) and strain (s) parameters along with the fractional coordinates are depicted in table 2 for o-$YMnO_3$ as well as $LaMnO_3$ and compared with the experimental [16, 30] and calculated results. Table 3 contains a selected list of bond distances and bond angles.

3.2. Raman and infrared frequencies

We report the Raman frequencies for $YMnO_3$ in its orthorhombic phase in table 4. The calculated phonon frequencies are in good agreement with the observed Raman data [19]. A comparison with the shell-model computation by Iliev *et al* [19] shows that the average deviation of the calculated Raman frequencies is 11.8%, whereas our present model gives this value as 7%. Also Iliev *et al* have used a

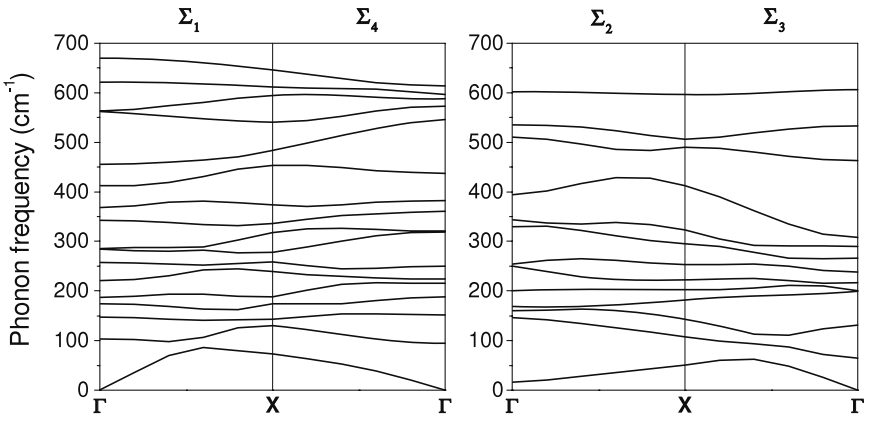

Figure 4. Computed phonon dispersion curves for o-$YMnO_3$ along the high symmetry Σ direction. Group theoretical representations are indicated on top of the figure. Γ is the Brillouin zone centre and X is the zone boundary.

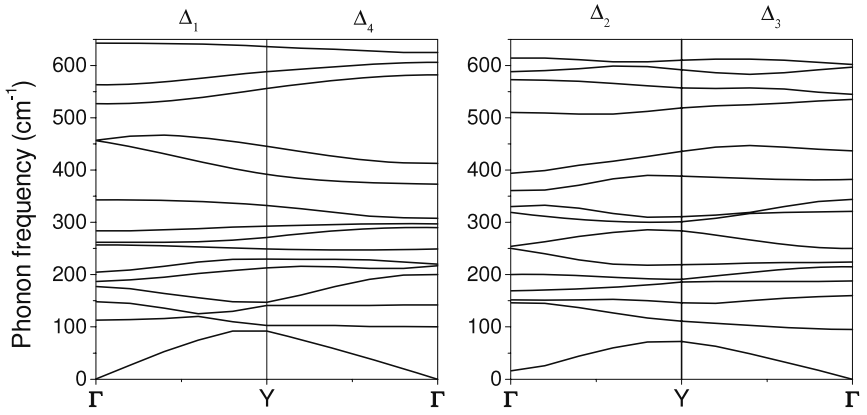

Figure 5. Computed phonon dispersion curves for o-$YMnO_3$ along the high symmetry Δ direction. Group theoretical representations are indicated at the top of the figure. Γ is the Brillouin zone centre and Y is the zone boundary.

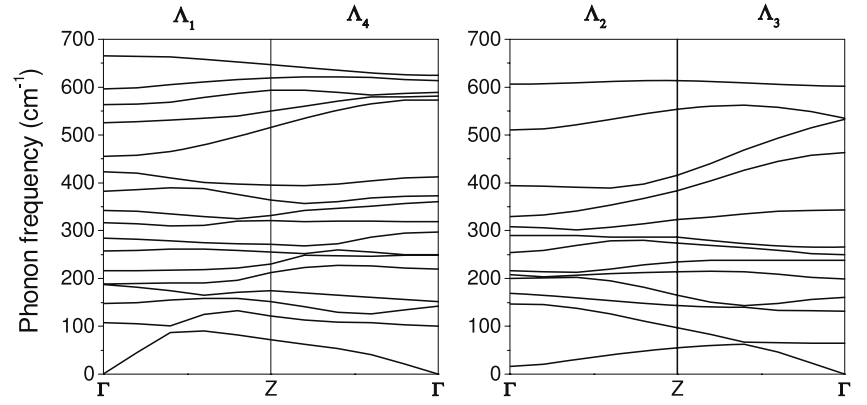

Figure 6. Computed phonon dispersion curves for o-$YMnO_3$ along the high symmetry Λ direction. Group theoretical representations are indicated at the top of the figure. Γ is the Brillouin zone centre and Z is the zone boundary.

much more complex model [19] with 20 parameters while our shell model has only seven parameters. Thus, all 24 Raman active modes ($7A_g + 5B_{1g} + 7B_{2g} + 5B_{3g}$) of vibrations listed in table 4 are found to compare well with experimental [19] data. An inspection of the eigenvectors of these modes shows that: (i) Mn does not participate in these Raman active modes, and (ii) the motions of Y and O1 atoms are restricted within the xz plane for the A_g and B_{2g} modes, and along the y-axis for the B_{1g} and B_{3g} modes.

The IR phonon spectrum for o-$YMnO_3$ can be classified into three phonon bands: the low frequency external phonon band (<290 cm^{-1}) (mainly due to Y and MnO_6 motions), the bending phonon band at intermediate range and the high frequency stretching band (>590 cm^{-1}). In the absence of any single crystal data, only the polycrystalline data of Subba Rao *et al* [25] are compared to our calculated results as depicted in figure 1.

Table 3. Comparison between the experimental [16, 30] and calculated (at 0 K) bond distances (Å) and selected angles (deg) for o-$LaMnO_3$ (experimental data [30] at 14 K) and $YMnO_3$ (experimental data [16] at 295 K).

	$LaMnO_3$		$YMnO_3$	
	Experimental [30]	Calculated [28]	Experimental [16]	Calculated (this work)
Mn–O1 (x2)	1.9646	1.997	1.9385	1.986
Mn–O2 (x2)	2.178	2.021	2.200	2.091
Mn–O2 (x2)	1.906	2.019	1.904	1.964
⟨Mn–O⟩	2.0178	2.012	2.014	2.014
Mn–O1–Mn (x2)	155.0	154.3	143.51	141.7
Mn–O2–Mn (x4)	154.84	153.4	144.55	142.7
⟨Mn–O–Mn⟩	154.89	153.8	144.20	142.2
R–O1	2.552	2.486	2.306	2.234
R–O1	2.420	2.394	2.252	2.198
R–O2 (x2)	2.646	2.671	2.501	2.525
R–O2 (x2)	2.445	2.394	2.303	2.236
R–O2 (x2)	2.698	2.719	2.553	2.632
⟨R–O⟩	2.569	2.556	2.409	2.402

Table 4. Comparison of the calculated Raman active phonon frequencies for o-$YMnO_3$ with the experimental Raman data [19] and other calculated results [19]. The vibrating atoms and the vibrational direction (in brackets) are indicated along with the mode assignment. Bend, tilt, rotation and stretch refer to the respective motions of the oxygen atoms in the MnO_6 octahedron in the unit cell.

Experimental [19]	Calculated shell model [19]	Calculated shell model (this work)	Largest atomic displacements/assignment (this work)
		A_g	
151	104	148	Y (x)
188	147	187	Y (z)
288	223	257	O2 (x, z)/rotation
323	304	284	Y (z)
396	407	343	O2 (x, y)/rotation
497	466	456	O2 (y, z)/bend
518	524	563	O1 (z)/stretch
		B_{1g}	
205	181	200	Y (y)
	288	217	O2 (x, z)/rotation
284	342	290	O2 (x, z)/rotation
383	413	308	O1 (y)/stretch
	593	606	O1 (y)/stretch
		B_{2g}	
151	137	153	Y (z)
220	162	250	Y (x)
317	285	319	O2 (y)/rotation
341	393	361	O2 (y, z)/rotation
481	470	573	O1 (x)/bend
537	583	588	O1 (x, z)/bend
616	617	614	O2 (y, z)/stretch
		B_{3g}	
178	145	160	Y (y)
	363	250	O2 (x, z)/rotation
336	390	344	O2 (y)/bend
	476	535	O2 (x, z)/bend
	610	602	O1 (y)/stretch

3.3. Phonon density of states and phonon dispersion relation

The computed phonon density of states for o-$YMnO_3$, as shown in figure 2, spans the spectral range from 0 to 85 meV. The density of states show a broad structure with peaks around 9, 19, 30, 52, 71 and 76 meV. Due to the partial structural disorder [31], the Raman spectra of doped rare earth manganites is expected to have bands of phonon density of states origin. In figure 2, the phonon density of states for o-$YMnO_3$, as obtained from lattice dynamics, is compared with the Raman spectra [31] of $Y_{1-x}Ca_xMnO_3$ ($x = 0.2$) in the configurations close to xx and xz.

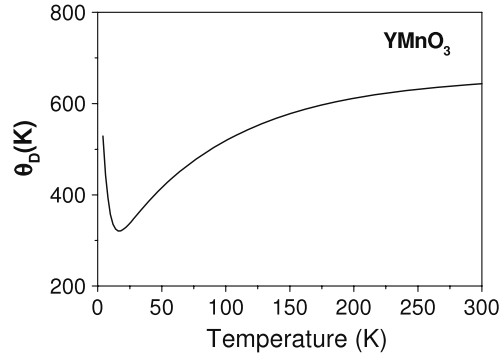

Figure 7. The variation of Debye temperature with temperature as obtained from present lattice dynamical calculations.

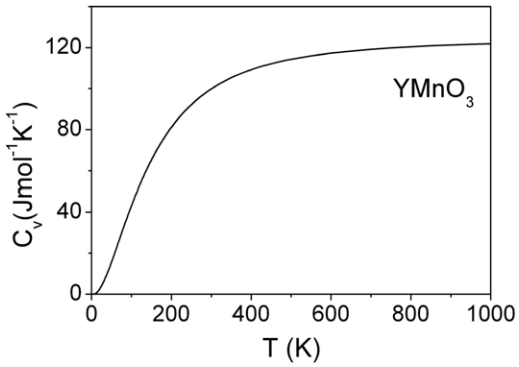

Figure 8. Calculated temperature dependence of specific heat of orthorhombic $YMnO_3$.

The calculated partial densities of states are shown in figure 3. The phonon vibrations due to Y, Mn and O atoms contribute in the entire 85 meV range. Y and Mn atoms largely contribute up to 45 meV. The peaks around 9, 19 and 30 meV are because of the vibrations of Y and Mn atoms, whereas the peaks at 52, 71 and 76 meV can be attributed to those from the O atoms.

The calculated phonon dispersion curves for $YMnO_3$ along the three high symmetry directions Σ, Δ and Λ in the Brillouin zone are shown in figures 4–6. The modes that belong to different representations are plotted separately in the same figures. With 20 atoms in the unit cell, the phonon dispersion relation has 60 phonon branches along each symmetry direction. At the zone boundary points X, Y and Z, the branches degenerate in pairs due to the high symmetry at these points. From the phonon dispersion curves, it is noticed that for o-$YMnO_3$, one A_u mode at the Γ point is much softer than seen in the phonon dispersion curves for $LaMnO_3$ [28]. This is a clear indication of the metastability of the orthorhombic phase of $YMnO_3$.

3.4. Debye temperature and specific heat

The variation of Debye temperature (Θ_D) with temperature is shown in figure 7. The Debye temperature varies from 320 to 644 K in the temperature range up to 300 K. In the low temperature range (up to 10 K) this calculated variation is in the range 357–529 K.

The temperature variation of the calculated specific heat at constant volume (C_V) for o-$YMnO_3$ in the temperature range $0\ \text{K} \leqslant T \leqslant 1000\ \text{K}$ is shown in figure 8. No experimental data are available for comparison.

4. Conclusions

This paper provides a microscopic interpretation of various properties related to the structure and dynamics of a complex material (perovskite $YMnO_3$) through a simple lattice dynamical model and succeeds in explaining the comparatively larger structural distortion of o-$YMnO_3$ with respect to that of $LaMnO_3$ as well as vibrational data of $YMnO_3$. The calculated crystal structure, Raman and IR frequencies are in good agreement with the experimental data. The potential model reproduces a crystal structure which agrees well with the reported bond lengths and bond angles as well as the distortion parameter both for lanthanum and yttrium manganite. Describing the structural and vibrational properties of complex perovskites like $YMnO_3$, using interatomic potentials is non-trivial, and the agreement from our calculations is very satisfactory. The effective charge on the oxygen ion in yttrium manganite needs to be higher than that in lanthanum manganite. This feature is in keeping with the more ionic character of this perovskite. Further, the model gives an indication of the observed metastability of yttrium through a softening of a silent phonon mode. Thus, this study of the lattice properties of orthorhombic manganites is leading to a consistent understanding of the vibrational and thermodynamic properties of these complex compounds.

Acknowledgments

One of the authors (NKG) is thankful to the University Grants Commission (UGC), New Delhi for financial support. The other author (NK) is thankful to the Department of Science and Technology, New Delhi for the award of Fast Track Research Award for this project work.

References

[1] Tokura Y, Tomioka Y, Kuwahara H, Asamitsu A, Morimoto Y and Kasai M 1996 *J. Appl. Phys.* **79** 5288
[2] Ramirez A P 1997 *J. Phys.: Condens. Matter* **9** 8171
[3] Hazama H, Nemoto Y, Goto T, Asamitsu A and Tokura Y 2000 *Physica* B **281/282** 487
[4] Yang Y-F and Held K 2007 *Phys. Rev.* B **76** 212401
[5] Wu L, Klie R F, Zhu Y and Jooss Ch 2007 *Phys. Rev.* B **76** 174210
[6] Mahendiran R, Tiwary S K, Raychaudhuri A K, Ramakrishnan T V, Mahesh R, Rangavittal N and Rao C N R 1996 *Phys. Rev.* B **53** 3348
[7] Moritomo Y, Asamitsu A, Kuwahara H and Tokura Y 1996 *Nature* **380** 141
[8] Kimura T, Tomioka Y, Kuwahara H, Asamitsu A, Tamura M and Tokura Y 1996 *Science* **274** 1698
[9] Shimakawa Y, Kubo Y and Manako T 1996 *Nature* **379** 53
[10] Cheong S W, Hwang H Y, Batlogg B and Rupp L W Jr 1996 *Solid State Commun.* **98** 163

[11] Coey J M D, Viret M and von Molnar S 1999 *Adv. Phys.* **48** 167 and references therein
[12] Jin S, Tiefel T H, McCormack M, Fastnacht R A, Ramesh R and Chen L H 1994 *Science* **264** 413
[13] Gilleo M A 1957 *Acta Crystallogr.* **10** 161
[14] Quezel S, Rossat-Mignod J and Bertaut E F 1974 *Solid State Commun.* **14** 941
[15] Khomskii D I and Sawatzky G A 1997 *Solid State Commun.* **102** 87
[16] Alonso J A, Martínez-Lope M J, Casais M T and Fernández-Díaz M T 2000 *Inorg. Chem.* **39** 917
[17] Muñoz A, Alonso J A, Casais M T, Martínez-Lope M J, Martínez J L and Fernández-Díaz M T 2002 *J. Phys.: Condens. Matter* **14** 3285
[18] Lorenz B, Wang Y Q, Sun Y Y and Chu C W 2004 *Phys. Rev.* B **70** 212412
[19] Iliev M N, Abrashev M V, Lee H G, Popov V N, Sun Y Y, Thomsen C, Meng R L and Chu C W 1998 *Phys. Rev.* B **57** 2872
[20] Martín-Carrón L, de Andrés A, Martínez-Lope M J, Casais M T and Alonso J A 2002 *Phys. Rev.* B **66** 174303
[21] Iliev M N, Abrashev M V, Popov V N and Hadjiev V G 2003 *Phys. Rev.* B **67** 212301
[22] Iliev M N, Abrashev M V, Laverdiere J, Jandl S, Gospodinov M M, Wang Y Q and Sun Y Y 2006 *Phys. Rev.* B **73** 064302
[23] Laverdiere J, Jandl S, Mukhin A A, Ivanov V Yu, Ivanov V G and Iliev M N 2006 *Phys. Rev.* B **73** 214301
[24] Gupta H C and Ashdhir P 1999 *Physica* B **262** 1
[25] Subba Rao G V, Rao C N R and Ferraro J R 1970 *Appl. Spectrosc.* **24** 436
[26] Kim J, Jung S, Park M S, Lee S I, Drew H D, Cheong H, Kim K H and Choi E J 2006 *Phys. Rev.* B **74** 052406
[27] Chen M, Hallstedt B and Gauckler L J 2005 *J. Alloys Compounds* **393** 114
[28] Rini E G, Rao M N, Chaplot S L, Gaur N K and Singh R K 2007 *Phys. Rev.* B **75** 214301
[29] Chaplot S L, Choudhury N, Ghose S, Rao M N, Mittal R and Goel P 2002 *Eur. J. Mineral.* **14** 291
Chaplot S L 1978 *External Report No.* BARC-972 Bhabha Atomic Research Centre, unpublished
[30] Huang Q, Santoro A, Lynn J W, Erwin R W, Borchers J A, Peng J L and Greene R L 1997 *Phys. Rev.* B **55** 14987
[31] Iliev M N, Lorenz B, Litvinchuk A P, Wang Y-Q, Sun Y Y and Chu C W 2005 *J. Phys.: Condens. Matter* **17** 3333